Numerical simulation of the motion of atmospheric fronts using a two layer model

By ARNE GRAMMELTVEDT, *Institute of Geophysics, University of Oslo*

(Manuscript received May 15, 1970; revised version September 1, 1970)

ABSTRACT

The equations describing a two-layer frontal model of the atmosphere, where all the baroclinicity is concentrated along a frontal surface separating two incompressible, homogeneous fluids in stable stratification, are integrated numerically. The upper boundary is a free surface, and the motion of the surface front at the lower boundary is found by calculating the trajectories of material "particles" on the surface front, using the known velocities in the grid points in the cold air layer. The development of frontal waves in the experiments showed a remarkable agreement with the development of observed frontal waves with the characteristic asymmetry between the warm and cold front side of the waves.

1. Introduction

The formation of fronts and the development of frontal cyclones in the atmosphere of the middle latitude were first described on the basis of synoptic investigations by the Bergen school in meteorology (Bjerknes & Solberg, 1922). They found that the typical cyclones originated as wave-like disturbances on the transition zone between the cold polar air mass and the warm tropical air mass; the polar front. Later Solberg (1928) treated theoretically the development of the frontal cyclones. He defined the front as a discontinuity surface between two statically stable, barotropic layers moving zonally with different velocities. To avoid the singularity connected with the intersection of the frontal surface with the ground, he assumed that the model was bounded by two sloping rigid planes, parallel to the frontal surface. By using the method of small perturbations he found two types of amplifying waves; one with very short wavelength (Helmholtz instability) and one with wavelength corresponding to the wavelength of observed young cyclones. It was originally believed that the shearing instability also was responsible for the growth of these long waves (Bjerknes & Godske, 1936), but later Høiland (1943, 1948) showed that long waves of the same nature as those found by Solberg may grow as a result of an interaction between the shear and the internal static stability of the two layers. Kotschin (1932) treated the frontal cyclone problem by assuming that the quasi-static approximation could be used. By considering two incompressible, homogeneous fluids with a shear and a density difference, bounded above and below by two rigid horizontal planes, he found by perturbation methods a stability criterion relating the shear and density difference between the two fluids to the wavelength. Eliasen (1960) simplified Kotschin's model by introducing a vertical wall at the northern boundary so that the frontal surface never intersected the upper surface. For particular values of the shear and density difference, corresponding to observed atmospheric conditions, he found the largest growth-rates for waves with wavelength approximately 2 000 km. The most extensive investigation of the instability of the frontal waves with the same model as Kotschin is recently done by Orlanski (1968). He found that in the region of Rossby number (Ro) $\leqslant 3$ and Richardson number (Ri) $\leqslant 5$ unstable waves may exist for all wavenumbers.

These linearized models give a relation between the initial growth of the unstable waves and the shear and density differences, but to study a more complete evolution of the frontal cyclones the non-linear effects of the dynamical equations have to be taken into account. This was done by Kasahara, Isaacson & Stoker (1965) in their numerical intergration of the development of a frontal cyclon in a two-layer model. But they made the simplification in the model that the warm air mass was inactive so the dynamics of the perturbations in the warm air layer could be neglected. Their system of differential equations could then be reduced to a set of only three prognostic equations.

In this study we will use the same model as Eliasen (1960) and as Kasahara et al. (1965), but the upper boundary of the warm air layer is a free surface. The intersection between the discontinuity surface and the lower boundary, the surface front, is treated as a free boundary as done by Kasahara et al., but the movement of this surface front is calculated by another method as discussed in section 4. The integration of the model is performed for three days of simulated time, and the surface frontal system is developing from a sinusoidal initial wave through the different stages of cold and warm fronts to an almost occluded frontal system.

2. The front model

We will consider a model consisting of two layers of incompressible homogeneous fluids with different densities. The motion in each layer is hydrostatic and independent of the vertical coordinate z. The two layers are bounded below with a rigid horizontal plane at $z=0$, and the upper limit of the fluids is a free surface at $z=h_2(x, y, t)$. The interface between the two layers, the frontal surface, is given by $z=h_1(x, y, t)$. The fluids are assumed confined in a channel corresponding to a middle latitude band on the earth. The southern and northern boundaries are rigid walls where the normal velocity components vanish, and it is assumed that the frontal surface never intersects with the free surface but ends on the northern wall. It is also assumed that the flow is periodic in the west-east direction with a periodicity equal to the length of the channel. The earth rotation is taken into account with a β-plan approximation.

Using a Cartesian coordinate system with the x-axis in the west-east and the y-axis in the south-north direction respectively, the equations in Eulerian from governing the model and which satisfy the dynamic and kinematic boundary conditions at $z=0$, h_1, and h_2 are as follows:

$$\frac{\partial \mathbf{v}_1}{\partial t} + \mathbf{v}_1 \cdot \nabla \mathbf{v}_1 + f\mathbf{k}x\mathbf{v}_1 + g\nabla h_1 + \frac{\varrho_2}{\varrho_1} g\nabla (h_2 - h_1) = 0 \quad (1)$$

$$\frac{\partial \mathbf{v}_2}{\partial t} + \mathbf{v}_2 \cdot \nabla \mathbf{v}_2 + f\mathbf{k}x\mathbf{v}_2 + g\nabla h_2 = 0 \quad (2)$$

$$\frac{\partial h_1}{\partial t} + \nabla \cdot (h_1 \mathbf{v}_1) = 0 \quad (3)$$

$$\frac{\partial (h_2 - h_1)}{\partial t} + \nabla \cdot ((h_2 - h_1)\mathbf{v}_2) = 0 \quad (4)$$

$\mathbf{v}_1$ and $\mathbf{v}_2$ are the velocity vectors in the cold and warm air layers respectively, f is the Coriolis parameter, g is the acceleration of gravity, and $\mathbf{k}$ is the vertical unit vector. The fluids are in stable stratification so the density ϱ_1 of the cold air layer is larger than the density ϱ_2 of the warm air layer. For a stationary front the system of equations may be reduced to the well-known Margules' formula for the slope of the front

$$\frac{dh_1}{dy} = \frac{f(\varrho_2 U_2 - \varrho_1 U_1)}{g(\varrho_1 - \varrho_2)} \quad (5)$$

where U_1 and U_2 are the uniform velocities in the positive x-direction in each of the layers (Fig. 1).

By multiplying equation (3) with ϱ_1 and (4) with ϱ_2 and integrating the equations over the domains σ_1 and σ_2 of the cold and warm air

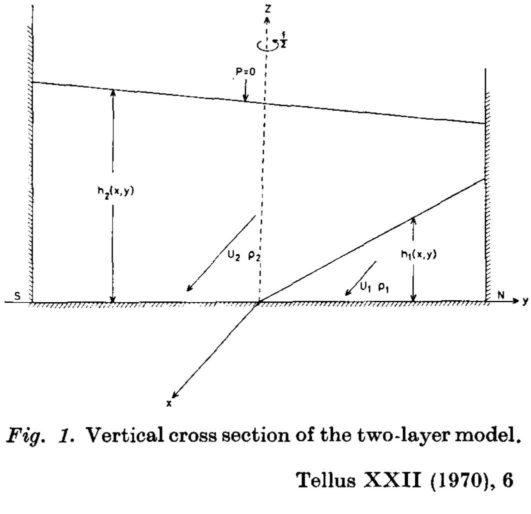

Fig. 1. Vertical cross section of the two-layer model.

masses respectively, and by using the boundary conditions, we see that the total mass of the cold air layer $M_1 = \varrho_1 \int_{\sigma_1} h_1 d\sigma$ and of the warm air layer $M_2 = \varrho_2 \int_{\sigma_2} (h_2 - h_1) d\sigma$ are conserved in the model. Likewise it is easy to show that the total energy

$$ET = \int_{\sigma_1} \varrho_1 \left(\frac{\mathbf{v}_1^2 + g h_1}{2}\right) h_1 \, d\sigma + \int_{\sigma_2} \varrho_2 \left(\frac{\mathbf{v}_2^2 + g(h_2 + h_1)}{2}\right) (h_2 - h_1) d\sigma \quad (6)$$

is conserved in the model.

We have as an upper boundary condition in this model used a free surface, but we may instead use a lid at $z = h_2 =$ constant. Instead of the continuity equation (4) for the warm air, we then have to solve a balance equation of the Monge-Ampère type for the pressure distribution at this upper boundary. But to solve numerically for each time step a Monge-Ampère equation is much more time consuming on the computer than integrating numerically the prognostic equation (4).

By using the same boundary conditions and the same linearizing procedure as Eliasen (1960), and also the approximations

$$\frac{\varrho_1}{\varrho_1 - \varrho_2} \simeq \frac{\varrho_2}{\varrho_1 - \varrho_2} = \frac{\bar{\varrho}}{\varrho_1 - \varrho_2}$$

the linearized set of equations corresponding to equation (1) to (4) reduce to the same equations as equations (3.12) and (3.13) in Eliasen's paper, where p_1^1 and p_2^1 have to be defined as

$$p_1^1 = \varrho_1 g \left[\left(1 - \frac{\varrho_2}{\varrho_1}\right) h_1 + \frac{\varrho_2}{\varrho_1} h_2\right]$$

and

$$p_2^1 = \varrho_2 g h_2$$

We have therefore to expect that the linear instability criterions for this model are the same as those found for Eliasen's model.

3. Finite difference equations and boundary conditions

The equations (1) to (4) will be integrated numerically by using one of the finite difference schemes (scheme F) discussed by Grammeltvedt (1969). In the calculations we will use a fixed regular grid with horizontal spacing $\Delta x = \Delta y = \Delta$ and with time increment Δt, and we will use the notations of Shuman (1962) where a second order finite difference approximation to the derivative of an arbitrary function α of a discrete variable $x_i = i\Delta$ is written

$$\frac{\partial \alpha}{\partial x} = \bar{\alpha}_x^x + 0(\Delta^2)$$

where

$$\bar{\alpha}^x = \frac{1}{2}\left(\alpha\left(x_i + \frac{\Delta}{2}\right) + \alpha\left(x_i - \frac{\Delta}{2}\right)\right)$$

and

$$\alpha_x = \frac{1}{\Delta}\left(\alpha\left(x_i + \frac{\Delta}{2}\right) - \alpha\left(x_i - \frac{\Delta}{2}\right)\right)$$

With these notations the finite difference equations for equations (1) to (4) may be written

$$\bar{u}_{jt}^{t} + (\bar{u}_j^x \bar{u}_j^x)_x + (\bar{v}_j^y \bar{u}_j^y)_y - u_j(\bar{u}_{jx}^y + \bar{v}_{jy}^y) - f v_j + \bar{\phi}_{jx}^x = 0 \quad (7)$$

$$\bar{v}_{jt}^{t} + (\bar{u}_j^x \bar{v}_j^x)_x + (\bar{v}_j^y \bar{v}_j^y)_y - v_j(\bar{u}_{jx}^x + \bar{u}_{jy}^y) + f u_j + \bar{\phi}_{jy}^y = 0 \quad (8)$$

$$\bar{h}_{1t}^{t} + (\bar{h}_1^x \bar{u}_1^x)_x + (\bar{h}_1^y \bar{v}_1^y)_y = 0 \quad (9)$$

$$\overline{(h_2 - h_1)}_t^t + (\overline{(h_2 - h_1)}^x \bar{u}_2^x)_x + (\overline{(h_2 - h_1)}^y \bar{v}_2^y)_y = 0 \quad (10)$$

for $j = 1, 2$.

$$\phi_1 = g\left(h_1 + \frac{\varrho_2}{\varrho_1}(h_2 - h_1)\right)$$

$$\phi_2 = g h_2$$

and u_j and v_j are the velocity components in the x and y directions respectively.

At the lower boundary the domain σ_1 of the cold air is restricted to the area between the northern wall and the surface front. This domain is changing during the development of the frontal cyclone through the changing position of the surface front and will not, from time step to time step, contain the same set of regular grid plints. It is therefore necessary to mark the set of regular grid points which at each time step belongs to the domain σ_1 of the cold air. In the regular grid points next to the surface front we cannot directly use the finite difference equations (7), (8), and (9), but we will approximate the spatial derivatives of the variables with non centered differences taken in the direction into the cold air.

There will also at the position of the surface front be a discontinuity in the gradient of the thickness of the warm air; $\nabla(h_2 - h_1)$. This discontinuity cannot directly be represented in the continuity equation (10), but it will introduce high wave number noise in the thickness field, which may be transfered to the velocity fields and make the integration computationally unstable. Therefore a Fickan type smoothing of the form $\mathbf{F} = \varkappa\nabla^2\mathbf{v}$, where $\varkappa$ is a turbulent diffusion coefficient, is introduced into the equations of motion (7) and (8), and the height fields h_1 and h_2 and the velocity fields are smoothed by a second order smoothing operator after each hour (18 step) of integration. Other experiments with primitive equation models have shown that it is probably better to suppress non-linear computational instability by including nop-linear friction terms in the equations as done by Smagorinsky, Manabe & Halloway (1965) or to use nine point formulas for the spatial derivatives, see Grammeltvedt (1969). But the changing position of the surface front and also the fact that regular grid points in the cold air layer next to the surface front do not have all their eight surrounding grid points inside the cold air region, makes it difficult to define non-linear operators or nine-point formulas in these grid points where the high wave number noise is strongest.

The lateral boundary conditions in the continuous model are that the velocity component normal to the boundaries is zero. But for the discrete model given by the finite difference equations (7)–(10) we have to impose two extra sets with boundary conditions, and we assume that also the first and second derivatives of the velocity component normal to the lateral boundaries are zero, i.e. $v = 0$, $\partial v/\partial y = 0$, and $\partial^2 v/\partial y^2 = 0$ at the lateral boundary. From these conditions follow that the velocity component u and the heights h_1 and h_2 are constant in time at the lateral boundaries if they initially are given a constant value along the boundaries.

4. The movement of the surface front

Kasahara et al. (1965) found the movement of the surface front by defining a string of material points on the front and calculated the motion of these points from a Lagrangian system of equations. In this study we will also define the surface front by a string of material points, but since these points constitute the free boundary of the *cold air layer*, the motion of these points will be found by calculating their trajectories by using the known velocities at the regular grid points of the cold air. We then avoid the difficulties in determining the gradients of h_1 at this free boundary. To make the calculation simple in this experiment we will as a first approximation define the velocity of a front point k at time $t = r + 1$ to be equal to the velocity at the nearest regular grid point in the cold air. This is done in the following way; let the coordinates of the front point k at time $t = r$ be $X^r(k)$ and $Y^r(k)$ in the basic coordinate system, and let i and j be the integers values of $X^r(k)$ and $Y^r(k)$. The front point is then situated between the regular grid points P_1, P_2, P_3, and P_4 (see Fig. 2) with coordinates i, j, $i+1, j$, $i+1, j+1$, and $i, j+1$. The nearest regular grid point to k in the cold air is here found to be P_4. The velocity components at time $t = r + 1$ are then, as a first approximation, set equal to

$$u_f^{r+1}(k) = u^{r+1}(i, j+1) \tag{11}$$

and

$$v_f^{r+1}(k) = v^{r+1}(i, j+1) \tag{12}$$

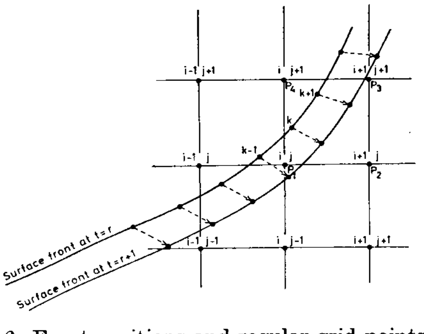

Fig. 2. Front positions and regular grid points.

From Fig. 2 follows that the front point $k+1$ also will get the same velocity as k, but the velocity of the front point $k-1$ will be set equal to the velocity at the regular grid point with coordinates $i-1$, j. This may give a very unsmoothed velocity distribution along the front. Therefore a second order smoothing operator is used along the front to smooth the velocities of the front points, and the final velocity components are then given as;

$$u^{r+1}(k) = \frac{1}{4}(u_f^{r+1}(k+1) + 2u_f^{r+1}(k) + u_f^{r+1}(k-1)) \quad (13)$$

and

$$v^{r+1}(k) = \frac{1}{4}(v_f^{r+1}(k+1) + 2v_f^{r+1}(k) + v_f^{r+1}(k-1)) \quad (14)$$

The new position of the front point k is then calculated by using a mean value of the velocity at time $t=r$ and $t=r+1$ which gives;

$$X^{r+1}(k) = X^r(k) + \frac{\Delta t}{2}(u^r(k) + u^{r+1}(k)) \quad (15)$$

$$Y^{r+1}(k) = Y^r(k) + \frac{\Delta t}{2}(v^r(k) + v^{r+1}(k)) \quad (16)$$

The new position of the surface front will change the domain σ_1 of the cold air, and the set of regular grid points which is included in σ_1 may therefore change from $t=r$ to $t=r+1$. A test is therefore made to determine if any regular grid points are located in the domain bounded by the surface front at $t=r$ and at $t=r+1$. If a regular grid point is included in the new domain σ_1 as P_1 at Fig. 2, the local velocity at this point is set equal to the velocity of the surface front, but the height h_1 is still set equal to zero. We are then introducing an error in h_1 which is depending on the velocity and the slope of the front and the time step. But with the time step used in this experiment ($\Delta t =$ 200 sec) this error is small (order 10 m in h_1). If a regular grid point is excluded from the domain σ_1 the velocity and the height h_1 are set equal to zero.

The calculation procedure to advance one time step can then be summarized as follows:

(a) The new values of the velocity and height fields in all regular grid points of the cold and warm air at time $t=r+1$ are determined from their values at time $t=r-1$ and $t=r$ using the *finite difference equations* (7) *to* (10).

(b) The new velocity of the front points at time $t=r+1$ are determined using the equations (11) to (14) and their new positions are found using the equation (15) and (16).

(c) A test is made to determine whether or not the set of regular grid points, which at each time step is inside the domain σ_1 of the cold air, has been changed from time $t=r$ to $t=r+1$. If a regular grid point is included in the new set, the local velocity in this grid point is defined to be that of the surface front, but the local height is still set equal to zero. If a regular grid point is excluded from the new set, its velocity and height are set equal to zero.

5. Initial conditions

The investigation by Eliasen (1960) showed that waves with wavelength approximately 2 000 km were the most unstable waves in his linearized model. We will therefore also in this model with a free surface choose an initial condition describing a westerly zonal flow with mean zonal velocity U and with north-south perturbations of wavelength 2 000 km. The height h_2 of the free surface is given as

$$h_2 = H_0 - U\left[f_0(y-y_0) + \frac{1}{2}\beta(y-y_0)^2\right] + H_1 \sin\frac{2\pi x}{L}\,\mathrm{sech}^2\frac{9(y-y_0)}{D} \quad (17)$$

where L is the length, and D is the width of the channel, and $y_0 = D/2$. The frontal surface is given in the same way as

$$h_1 = U_f(f_0(y-y_0) + \frac{1}{2}\beta(y-y_0)^2) + H_2 \sin\frac{2\pi(x+\delta)}{L}\,\mathrm{sech}^2\frac{9(y-y_0)}{D} \quad (18)$$

where δ is a phase displacement between the perturbation of the front and of the free surface, and U_f determines the slope of the frontal surface.

In the numerical calculation the following values of the parameters are adopted

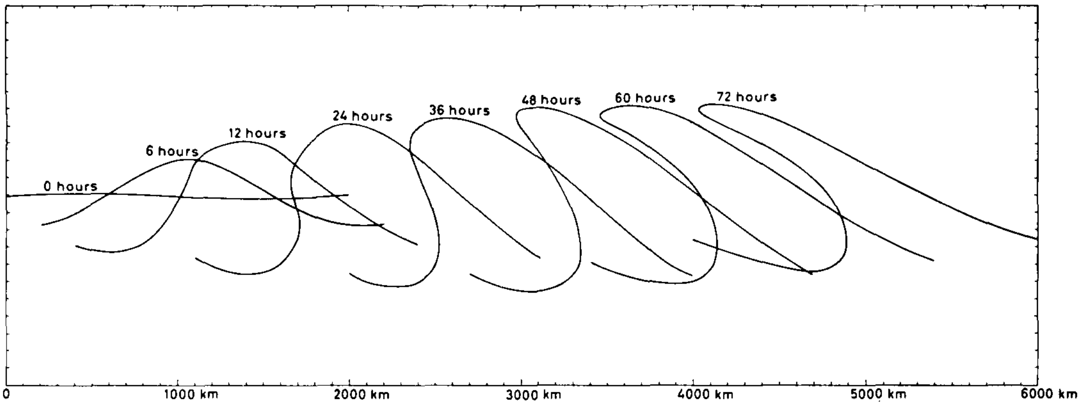

Fig. 3. The position of the surface front at 12 hours interval from initial time up to 72 hours of simulated time.

$H_0 = 8\,000$ m
$H_1 = 40$ m
$H_2 = 0$
$\delta = 0$
$U = 20$ m sec^{-1}

$U_f = 600$ m sec^{-1}
$L = 2\,000$ km
$D = 2\,200$ km
$f_0 = 10^{-4}$ sec^{-1}
$\beta = 1.5\ 10^{-11}$ sec^{-1} m^{-1}
$g = 10$ m sec^{-2}
$\varrho_1 = 1.25$ kg m^{-3}
$\dfrac{\varrho_2}{\varrho_1} = 0.98$

With this value of U_f the slope of the frontal surface is of the order 10^{-2}, and the density difference between the cold and warm air layers corresponds to a temperature difference of 6°K. The initial height fields h_1 and $h_2 - H_0$, and the pressure field at the lower boundary, $z = 0$,

$$p_s = g\varrho_1 h_1 + g\varrho_2(h_2 - h_1)$$

are given in Fig. 4. The initial velocity fields are calculated from the geostrophic approximation, and a turbulent diffusion coefficient $\varkappa = 7.5 \times 10^3$ m^2 sec^{-1} is used.

We have here given initially only a perturba tion in the height field h_2 of the free surface and no perturbation of the frontal surface. Experiments with initial perturbations in the height fields of both surfaces and also with perturbations only in the height field h_1 of the frontal surface, gave almost the same development of the frontal wave.

6. Result

The model is integrated with a basic grid of 20×23 grid points in the west-east and south-north directions respectively ($\Delta = 100$ km) and with a time step $\Delta t = 200$ sec. The surface front is represented by 80 material points, which initially are uniformely distributed along the front with equal spacing in the x-coordinate direction, i.e. it is initially four material front points between each regular grid point. With the initial conditions given in the previous section the model was integrated for more than three days of simulated time, and Fig. 3 shows the position of the surface front at 12 hours interval from initial time up to 72 hours following one particular frontal wave or cyclone. We see that the frontal wave is developing from an almost sinusoidal form at 6 hours, to an almost occluded wave at 72 hours. Because of the second order smoothing along the front of the velocity of the front points, the surface front itself has also to be a smooth curve, and we can therefore not expect to find a sharp occlusion point in this model with a discontinuity in the tangential direction of the front.

Figs. 4 and 5 show the pressure fields p_s at $z = 0$, the height fields h_1 of the frontal surface, and the height fields h_2 of the free surface at initial time and after 12, 36 and 72 hours of simulated time. We see that during the development of the frontal wave the pressure in the center of the surface cyclone is falling slowly from approximately 995 mb initially to 984 mb after 72 hours. The strongest deepening took place in the first 24 hours when the pressure fell to 988 mb; later the deepening is very slow. This comes probably from the strong smoothing of the velocity fields and of the

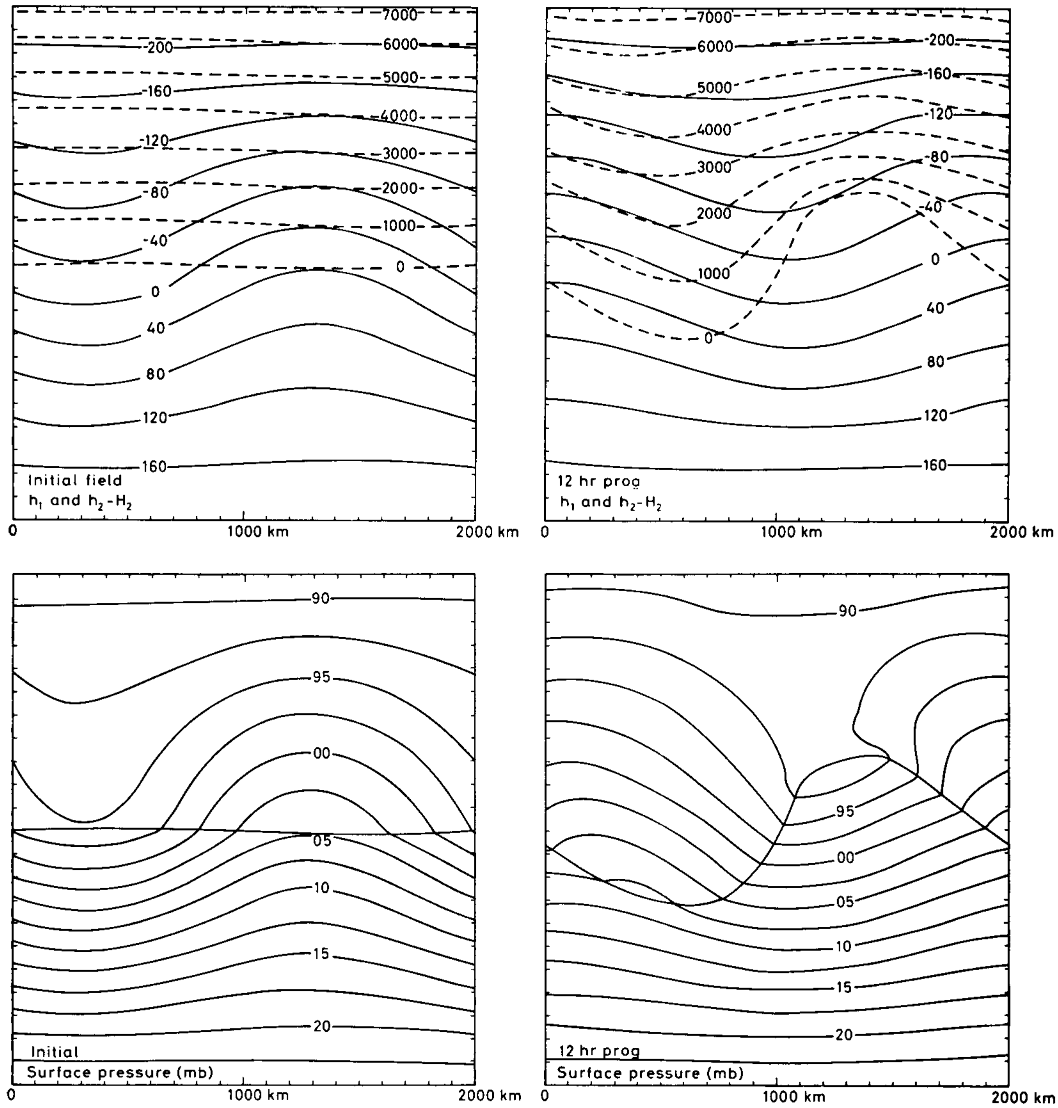

Fig. 4. Above: the height fields h_1 of the frontal surface (---) and the height fields $h_2 - H_2$ of the free surface (—) in meters. Below: the surface front and the surface pressure field. p_s in mb. All at initial time and after 12 hours of simulated time.

height fields which was introduced to get the integration numerically stable. From Fig. 5 we see that already after 36 hours the upper trough is weakened and after 72 hours there is only a very weak trough to the west of the surface pressure low.

We also see that the warm front in this model is much steaper than the cold front, which is contradictory to what is observed in real frontal cyclones. In this model the cold air behind the surface cold front consists only of a relatively thin layer penetrating underneath the warm air layer.

In Fig. 3 we were following one particular frontal wave, but since the model is periodic in the west-east direction the surface fronts associated with this frontal wave do not consist of the same set of front points (because of

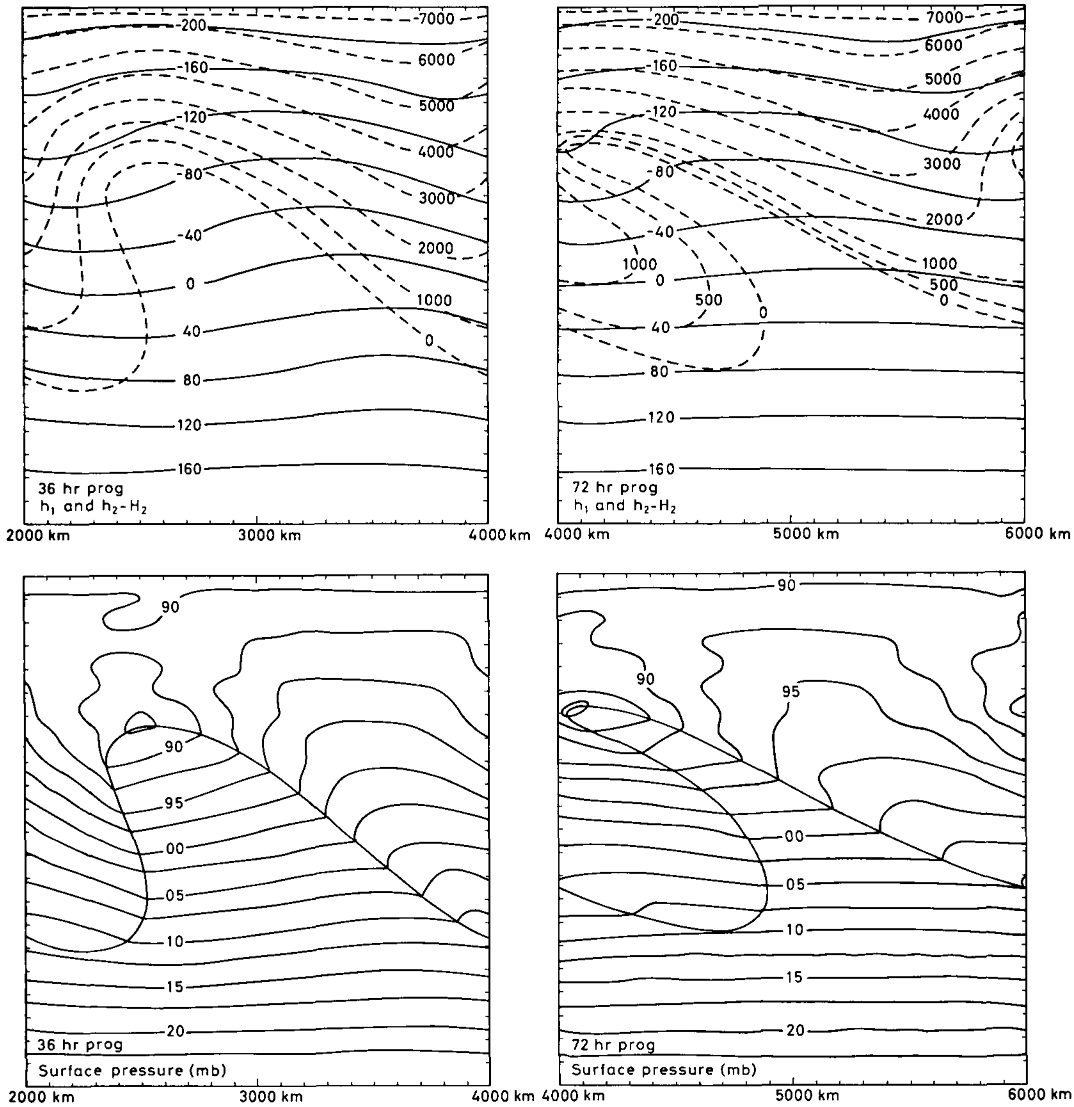

Fig. 5. The same as Fig. 4, but after 36 and 72 hours of simulated time.

the periodicity there is always 80 points inside a frame of 21×23 grid points), but we find that the wave is moving faster than the individual particles. In Fig. 6 is given the initial position and the positions after 24, 48, and 72 hours of the particular set of front points which initially constituted the surface front in Fig. 4. The position of five individual front points, which initially are uniformally separated with a distance L/4, are marked specificly. We notice that during the development of the frontal wave, the front is stretched considerably. The stretching is strongest along the warm front which can be seen from the increased distance between the points 4 and 5 at 24 hours, between 1 and 2 at 48 hours, and between 2 and 3 at 72 hours (Fig. 6). When the individual front points are passing from the warm front to the cold front side of the frontal wave, the distance between the front points are again decreasing.

When the surface front is stretched, the distance between two neighbouring front points can become very large, but to make the nu-

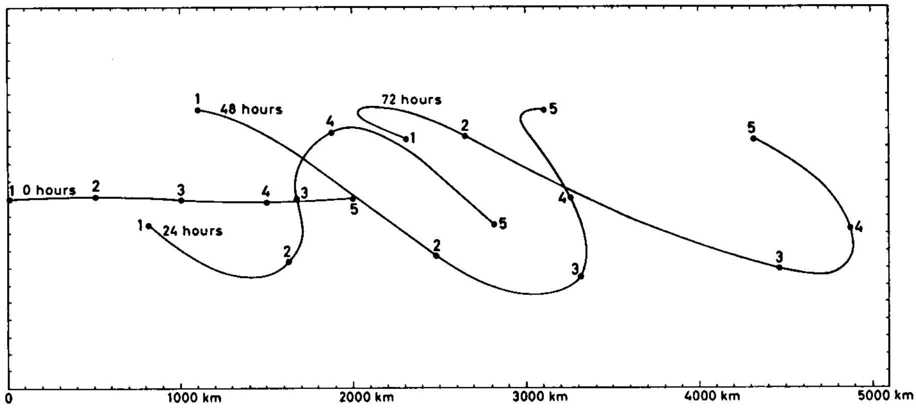

Fig. 6. The initial position and the position after 24, 48, and 72 hours of simulated time of the particular set of front points which initially constituted the surface front in Fig. 4. Five individual front points are marked specificly.

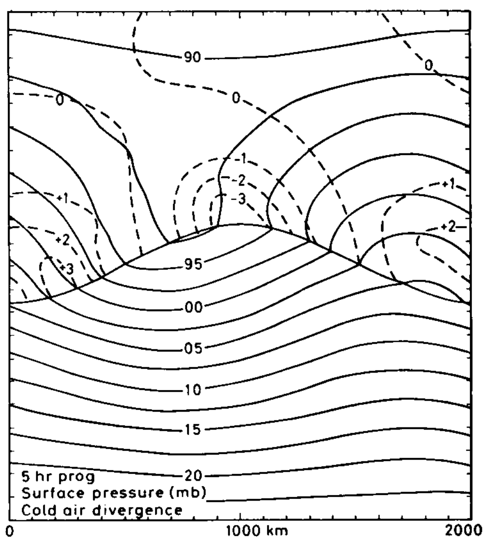

Fig. 7. The surface pressure field p_s (in mb) and the horizontal divergence $D_1 = (\partial u_1/\partial x) + (\partial v_1/\partial y)$ (unite 10^{-5} sec^{-1}) after 5 hours of simulated time.

merical procedure simple it was found to be necessary that the coordinate differences between two neighbouring front points k and $k+1$ at each time step were less or equal to the grid increment Δ, i.e.

$$|X^r(k+1) - X^r(k)| \leqslant \Delta$$

and (19)

$$|Y^r(k+1) - Y^r(k)| \leqslant \Delta$$

If the equations (19) are not fulfilled, the integration has to be terminated, or we have to redefine the set of front points so that equation (19) is fulfilled before the integration can continue. If we initially are defining a sufficiently large number of front points, the integration can run for a long time before it is necessary to redefine the set of front points. This model with a set of 80 front points was integrated for more than 80 hours of simulated time before the coordinate differences between two neighbouring front points became larger than the grid increment.

The vertical velocity at a height z in the cold air layer may be determined from the continuity equation (3), which gives

$$w_1 = -z\left(\frac{\partial u_1}{\partial x} + \frac{\partial v_1}{\partial y}\right)$$

In Fig. 7 is given the horizontal divergence $D_1 = (\partial u_1/\partial x) + (\partial v_1/\partial y)$ in the cold air together with the surface pressure field p_s after 5 hours of simulated time. We find as expected the strongest convergence area and the upward vertical velocity at the warm front side of the frontal wave and the corresponding divergence area and downward vertical velocity at the cold front side of the wave, but close to the ridge in the surface pressure field. The maximum vertical velocity at the frontal surface after 5 hours is approximately 5 cm sec^{-1}. Later the value of the horizontal convergence is increasing a little and the vertical velocity reaches the maximum of 8 cm sec^{-1}. The convergence area in the lower cold air layer has a corresponding compensating divergence area in the upper warm air layer, but the divergence area has a small displacement to the east in accordance with the results found in Eliasen's linearized model.

There are two serious objections to this model, and they are: the surface front is moved without taken into account that the total mass of the cold air and of the warm air should be conserved separately in the model, and the smoothing of the height fields h_1 and h_2 has a tendency to reduce the cold air mass and by that increase the warm air mass. In this experiment the cold air mass was very constant during the first day of integration, but later there was a slight decrease in the cold air mass, and after 3 days it had decreased with almost 4%, and there was a corresponding increase of the warm air mass. The total mass of the cold air is calculated by using the trapezoidal formula, and some of the variation in the calculated total mass may come from inaccuracy in using the trapezoidal formula when the frontal surface becomes more folded and when the domain σ_1 of the cold air is increasing.

Because of the smoothing used in the model the total energy is decreasing with time, but except for the first few hours the total energy is decreasing more than the kinetic energy, which shows that there is an over all transformation of potential energy to kinetic energy in the model.

6. Summary and conclusions

In this experiment a simplified two layer frontal model, where the baroclinicity is concentrated along the frontal surface, separating two homogeneous barotropic layers, is integrated numerically, but to keep the integration non-linearly stable a relatively strong dissipation and smoothing had to be introduced into the calculation.

The development of the surface frontal wave showed a remarkable agreement with the development of observed frontal waves with the characteristic asymmetry between the warm and cold front sides of the waves. But with the numerical method used in the calculation it was not possible to reach a stage of a completely occluded frontal wave.

The strongest convergence area and upward vertical velocity in the cold air layer is found at the warm front side of the surface frontal wave, and a corresponding divergence area and downward vertical velocity at the cold front side. The convergence area in the lower cold air layer has a compensating divergence area in the upper warm air layer, but it is shifted a little to the east in the same way as found in Eliasen's linearized model.

All the baroclinicity in this model is concentrated along the frontal surface and any perturbation in the cyclonic shear velocity or the horizontal pressure field (the velocity is initially calculated from the geostrophic equation) of a given wavelength will form a growing frontal wave. In this experiment therefore a perturbation only in the height field of the free surface was given initially. Other experiments with initial perturbation in the height fields of both surfaces and also experiments with perturbations only in the height fields of the frontal surface gave almost the same evolution of the surface frontal wave.

REFERENCES

Bjerknes, J. & Godske, C. L. 1936. On the theory of cyclone formation at extra-tropical fronts. *Astrophysica Norvegica 1*, 199–235.

Bjerknes, J. & Solberg, H. 1922. Life cycle of cyclones and the polar front theory of atmospheric circulation. *Geofysiske Publikasjoner*, vol. 3, no. 1. 18 pp.

Eliasen, E. 1960. On the initial development of frontal waves. *Publikationer fra Det Danske Meteorologiske Institut*, no. 13. 107 pp.

Grammeltvedt, A. 1969. A survey of finite differrence schemes for the primitive equations for a barotropic fluid. *Monthly Weather Review 97*, 384–404.

Höiland, E. 1943. On the wave motions in sliding layers with internal static stability. *Archiv for Mathematik og Naturvidenskap*, vol. 47, no. 3. 32 pp.

Höiland, E. 1948. Stability and instability waves in sliding layers with internal static stability. *Archiv for Mathematik og Naturvidenskap*, vol. 50, no. 3. 24 pp.

Kasahara, A., Isaacson, E. & Stoker, J. J. 1965. Numerical studies of frontal motion in the atmosphere. I. *Tellus 17*, 261–276.

Kotschin, N. 1932. Über die Stabilität von Margulesschen Diskontinuitätsflächen. *Beiträge zur Physik der freien Atmosphäre 18*, 129–164.

Orlanski, I. 1968. Instability of frontal waves. *Journal of the Atmospheric Science 25*, 178–200.

Shuman, F. G. 1962. Numerical Experiment with the Primitive Equations. Proceedings of the International Symposium on Numerical Weather Prediction in Tokyo, November 1960, pp. 85–107. Meteorological Society of Japan, Tokyo.

Smagorinsky, J., Manabe, S. & Halloway, I. L., Jr. 1965. Numerical result from a nine-level general circulation model of the atmosphere. *Monthly Weather Review 93*, 727–768.

Solberg, H. 1928. Integrationen der Atmosphärischen Störungsgleichungen. *Geofysiske Publikasjoner*, vol. 5, no. 9. 120 pp.

ЧИСЛЕННОЕ МОДЕЛИРОВАНИЕ ДВИЖЕНИЯ АТМОСФЕРНЫХ ФРОНТОВ НА ОСНОВЕ ДВУХУРОВЕННОЙ МОДЕЛИ

Численно интегрируются уравнения двухуровенной фронтальной модели атмосферы, в которой вся бароклинность сконцентрирована на фронтальной поверхности, отделяющей две несжимаемые однородные жидкости, устойчиво стратифицированные. Верхняя граница представляет собой свободную поверхность, а движение фронтальной поверхности на нижней границе находится вычислением траекторий материальных «частиц» на фронтальной поверхности по известным скоростям в точках сетки в слое холодного воздуха. Эволюция фронтальных волн в эксперименте обнаруживает замечательное согласие с эволюцией наблюдаемых фронтальных волн с характерной асимметрией между теплой и холодной сторонами фронтальной волны.